OE Optical Engineering

RESEARCH PAPER

Thermodynamic damage behavior of single-crystal MgF_2 irradiated by high-power fiber laser

Jiamin Wang,[a,b] Kuo Zhang,[a] Jinghua Yu,[a,b] Yi Chen,[a] Changbin Zheng,[a] Peng Yang,[c] Guohui Bao,[d] and Fei Chen[a,*]

[a]Changchun Institute of Optics, Fine Mechanics and Physics, Chinese Academy of Sciences, State Key Laboratory of Laser Interaction with Matter, Changchun, China
[b]University of Chinese Academy of Sciences, Beijing, China
[c]The First Representative Office of the Shenyang Military Representative Bureau of the Army Equipment Department in Changchun Region, Changchun, China
[d]Key Laboratory of Optoelectronic Countermeasures Testing and Evaluation Technology, Changchun, China

ABSTRACT. Magnesium fluoride (MgF_2) is a widely used optical window material in lasers. Laser-induced damage in MgF_2 materials involves complex thermal-mechanical coupling issues. With the rapid development of high-power fiber laser technologies and application of optoelectronic countermeasures, it is necessary to investigate the damage mechanism of 1.06 μm high-power continuous-wave laser on MgF_2 optical windows to clarify the laser damage threshold and factors influencing laser-irradiated MgF_2 window mirrors. Therefore, based on the theory of heat conduction and elastic mechanics, a simulation study was conducted using the finite element method. First, based on the thermo-mechanical theory, established a thermo-mechanical damage model for a laser-irradiated MgF_2 crystal. Second, we calculated the temperature, stress, and strain fields of single-crystal MgF_2 material under the action of a 100 W/cm^2 laser. When the laser was irradiated for 4.921 s, thermal stress-induced burst damage was observed, but no melting damage occurred. Finally, the impact of parameters such as the laser power density, spot size, and laser action time on the damage effect was discussed using the parametric scanning method. The calculation results showed that the aforementioned factors significantly impact the damaging effect. Moreover, under the same laser parameters, material burst due to thermal stress is expected to precede the melt damage.

Keywords: high power fiber laser; MgF_2; finite element simulation; thermal stress; temperature

Paper 20221408G received Dec. 7, 2022; revised Jul. 25, 2023; accepted Aug. 2, 2023; published Sep. 6, 2023.

1 Introduction

The window mirror and fairing are the key components to ensure the regular operation of infrared optical systems, such as infrared imaging and infrared guidance. In addition to being affected by harsh environments, they may also face the risk of laser damage during actual use. Therefore, it is necessary to study the damage of laser to window mirror materials. MgF_2 single crystals, as a common window material, exhibit high hardness, stable chemical properties, and resistance to mechanical and thermal shock damage.[1] They are an excellent optical material with good light transmission performance in the wavelength range of 0.11 to 8.5 μm, birefringence properties, and high laser damage threshold.[2] With the development of high-power fiber laser technology, the interaction between intense laser and window materials has become a research hotspot.[3–10]

*Address all correspondence to Fei Chen, feichenny@126.com

0091-3286/2023/$28.00 © 2023 SPIE

There are many factors that affect the damage effect of laser on MgF_2, such as laser intensity, spot size, laser wavelength, and so on.[11] The effect of different types of lasers on magnesium fluoride is quite different. Liu et al.[12] conducted an experimental study on the laser irradiation of MgF_2 polycrystals under different powers and pulse parameters and found that when the MgF_2 polycrystalline structure is subjected to a low-power long-pulse laser, the sintering and thermal stress lead to microcracks on the cleavage surface of the target. Qi et al. used a 10.6 μm CO_2 continuous laser to conduct an experiment on the irradiation effect of MgF_2 materials and found that under certain power density, MgF_2 materials can be destroyed at the fastest speed.[13] Wang et al.[14] numerically simulated the temperature and stress-strain fields of a fluorine glass window irradiated by a 3.8 μm hollow rectangular laser beam. Sun et al.[15] studied single-shot damage in MgF_2 irradiated by an 800 nm femtosecond laser and found that both multiphoton and avalanche ionization play an important role in femtosecond laser-induced damage in MgF_2. Lou et al.[16] explored the thermodynamic damage mechanism caused by pollutants, and numerically simulated the temperature and stress fields of optical components irradiated by a 3.8 μm hollow rectangular high-power continuous wave (CW) laser. Kato et al.[17] used the laser-induced deflection method to measure the absorption rate of MgF_2 materials at a laser wavelength of 193.4 nm. Andrus et al. experimentally studied the thermal lensing effect and nonlinear refractive index of MgF_2 crystal materials under a 1035 nm high-power ultrafast laser.[18] Migal et al.[19] established a laser-induced electron dynamics model based on the rate equation to explore the dependence of threshold on the wavelength of plasma formation under a high-power mid-infrared laser. In the aforementioned studies, mid-infrared and ultraviolet lasers were used as the light source for irradiation. However, few studies have analyzed the damage caused in MgF_2 windows by 1.06 μm CW laser in the near-infrared band.

Thus, with the development of high-power laser technologies, it is important to study the damage mechanism and threshold of MgF_2 windows by the irradiation of high-power lasers in the near-infrared band. In addition, there is a problem of high efficiency and cost ratio in laser damage experiment, so a theoretical model is urgently needed to predict and evaluate near-infrared laser damage to MgF_2. Our laboratory has already conducted research on the damage caused by high-power lasers on window materials.[20–22] In this study, heat conduction and elastic mechanics were used to couple solid heat transfer and solid mechanics. The finite element method was used to numerically simulate the thermodynamic damage behavior of a single-crystal MgF_2 window by a high-power fiber laser. The simulation results showed the temperature and stress field distributions of MgF_2 under different laser and material parameters. Accordingly, the damage characteristics of MgF_2 window mirrors under near-infrared laser irradiation were revealed, which can provide a reference for high-power laser irradiation optical window materials.

2 Theory

In the laser irradiation of MgF_2 window lens, first, the laser is incident on the material surface vertically; then, the part irradiated by the laser absorbs the laser energy and gets transferred to the inside of the material through thermal conduction. When the thermal stress exceeds the breaking strength of the material, the material bursts; moreover, when the surface temperature reaches the melting point, the material melts. Owing to the complex thermomechanical coupling mechanism, the thermodynamic parameters of the material change during laser action; therefore, the analytical solution can only be replaced by the numerical solution of temperature and stress. Based on the theory of heat conduction and elastic mechanics, we conducted a numerical simulation study on an MgF_2 window mirror irradiated by a single-mode Gaussian CW laser with a central wavelength of 1.06 μm; Fig. 1 shows the physical model. In this study, we focused on a single crystal hot-pressed MgF_2 window lens (without surface coating). In Fig. 1, the white area represents the Gaussian continuous laser irradiated at the center of hot-pressed MgF_2 ($\Phi 100$ mm $\times$ 4 mm) window lens. The material surface absorbs the laser energy and conducts heat radially and axially along the temperature gradients. Fixed constraints were applied on the sides of the window mirror to simulate window mirror clamping.

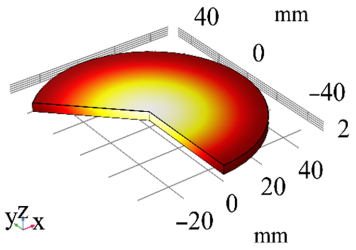

Fig. 1 Laser irradiation MgF_2 material model diagram.

2.1 Temperature Field

In the process of CW laser irradiation, to clarify the temperature change in the MgF_2 window mirror, a temperature field model was established for the MgF_2 material according to the heat conduction equation, presented in Eq. (1), where ρ, Cp, and k denote the density, constant pressure heat capacity, and thermal conductivity of single-crystal MgF_2, respectively; Q denotes the bulk heat source generated by laser power deposition in the material.

To effectively obtain the numerical solution of Eq. (1), its initial temperature, T_0, was set to be 293.15 K; moreover, thermal radiation and thermal convection, represented by Eqs. (3) and (4), respectively, were considered. Then, the corresponding boundary conditions were defined for the surface, Σ_2, irradiated by the laser. Equation (5) presents the heat source term. The Gaussian body heat source was multiplied by the time function, $g(t)$, to control the laser action time, where R, P, r_0, and α denote the reflectivity, laser power, spot radius, and absorption coefficient, respectively. The function of laser action time can be given by Eq. (6)

$$\rho C_p \frac{\partial T}{\partial t} - k\nabla^2 T = Q, \tag{1}$$

$$T|_{t=0} = T_0 = 293.15K, \tag{2}$$

$$-k\frac{\partial T}{\partial n}\bigg|_{\sum_1} = -hT - \varepsilon(T^4 - T_0^4). \tag{3}$$

$$-k\frac{\partial T}{\partial n}\bigg|_{\sum_2} = -hT, \tag{4}$$

$$Q = (1-R)\frac{p}{\pi r_0^2}\exp\left(-\frac{x^2+y^2}{r_0^2}\right)\cdot\alpha\cdot\exp(-\alpha\cdot z)\cdot g(t), \tag{5}$$

$$g(t) = \begin{cases} 1 & 10s \le t \le 10s + t_0 \\ 0 & 0s < t < 10s, 10s + t_0 < t < 60s \end{cases}. \tag{6}$$

2.2 Stress Field

When the laser action time is increased, the accumulated heat is absorbed by the material to generate thermal stress. We solved the elastic mechanics equation to clarify the thermodynamic damage effect of CW laser on MgF_2. First, the relationship between stress components was characterized by a balanced differential equation, presented in Eq. (7), where σ_x, σ_y, and σ_z denote the positive stress in the x, y, and z directions, respectively. Moreover, τ_{yx}, τ_{yz}, τ_{zx}, τ_{zy}, τ_{xz}, and τ_{xy} represent the shear stress. The displacement method was used to solve the aforementioned equation by eliminating the stress component; then, combining with the heat conduction theory, the equilibrium differential equation under variable temperature was obtained in the following equations:

$$\begin{cases} \frac{\partial \sigma_x}{\partial x} + \frac{\partial \tau_{yx}}{\partial y} + \frac{\partial \tau_{zx}}{\partial z} = 0 \\ \frac{\partial \sigma_y}{\partial y} + \frac{\partial \tau_{xy}}{\partial x} + \frac{\partial \tau_{zy}}{\partial z} = 0 \\ \frac{\partial \sigma_z}{\partial z} + \frac{\partial \tau_{xz}}{\partial x} + \frac{\partial \tau_{yz}}{\partial y} = 0, \end{cases} \tag{7}$$

$$\begin{cases} G\nabla^2 u_x + (K+G)\frac{\partial \theta}{\partial x} - \frac{\beta E}{1-2\mu}\frac{\partial T}{\partial x} = 0 \\ G\nabla^2 u_y + (K+G)\frac{\partial \theta}{\partial y} - \frac{\beta E}{1-2\mu}\frac{\partial T}{\partial y} = 0 \\ G\nabla^2 u_z + (K+G)\frac{\partial \theta}{\partial z} - \frac{\beta E}{1-2\mu}\frac{\partial T}{\partial z} = 0, \end{cases} \tag{8}$$

$$K = \frac{\mu E}{(1+\mu)(1-2\mu)}, \tag{9}$$

$$G = \frac{E}{2(1+\mu)}, \tag{10}$$

where μ, E, and β denote Poisson's ratio, elastic modulus, and thermal expansion coefficient, respectively, and G is the shear elastic modulus of the material. u_x, u_y, and u_z denote the displacement in the x, y, and z directions, respectively. ε_x, ε_y, and ε_z represent the positive strains of x, y, and z, respectively. The total positive strain, θ, can be represented by Eq. (11). The initial conditions are presented in Eqs. (12) and (13); a fixed constraint was imposed on the side tri-sector point, r', of the cylindrical model. The boundary conditions are shown in Eq. (14); the remaining interfaces are free interfaces

$$\theta = \varepsilon_x + \varepsilon_y + \varepsilon_z, \tag{11}$$

$$u_x|_{t=0} = 0,\ u_y|_{t=0} = 0,\ u_z|_{t=0} = 0, \tag{12}$$

$$\left.\frac{\partial u_x}{\partial t}\right|_{t=0} = 0,\ \left.\frac{\partial u_y}{\partial t}\right|_{t=0} = 0,\ \left.\frac{\partial u_z}{\partial t}\right|_{t=0} = 0, \tag{13}$$

$$u|_{r'} = 0. \tag{14}$$

3 Simulation

3.1 Parameter Determination

Table 1 and Fig. 2 list the critical parameters involved in the simulation calculation process. We considered the transformation relationship between the characteristic parameters of MgF_2 materials and temperature in the simulation. Moreover, the built-in MgF_2 parameters of the material library were used to characterize the thermodynamic parameters as a function of temperature.

We used the finite element method to simulate the optical window prepared by irradiating the MgF_2 material with a high-power fiber laser. The window was shaped like a cylinder (Φ100 mm $\times$ 4 mm); a Gaussian laser with a light spot of Φ20 mm acted on the window surface. During the meshing process, to improve the accuracy and convergence of calculation, a free quadrilateral mesh was used to mesh the material surface. Then, the entire mesh was meshed via sweeping, and the number of elements along the thickness direction was set to seven layers. The mesh division is shown in Fig. 3, where the maximum and minimum mesh elements are 6 and 0.54 mm, respectively.

4 Results and Discussion

4.1 Simulation Results

A single-crystal MgF_2 window mirror with a thickness and diameter of 4 and 100 mm, respectively, was irradiated with a 1.06 μm continuous laser (laser power: 1256.6 W, spot radius: 20 mm) for 10 s to better understand the time-dependent relationship between sample temperature and stress during laser irradiation. The observation and laser action time were 60 and 10 to 20 s, respectively.

Table 1 Key parameters in the simulation process.

Parameter	Symbol	Value
Laser wavelength (nm)	λ	1064
Laser power (W)	P	1256.6, 2513.3, 3769.9
Spot radius (mm)	r_0	10, 20, 30, 50
Surface emissivity	ε	0.3
Convective heat transfer coefficient $W/(m^2 \cdot K)$	h	10
Poisson's ratio	nu	0.278
Tangential thermal expansion coefficient (1/K)	Γ	13.7×10^{-6}
Absorption coefficient (m^{-1})	A	260
Reflectivity	R	0.03
Action time (s)	t_0	10, 20, 30
Young's modulus /(GPa)	E	138.5
Density (g/cm^3)	ρ	3.16

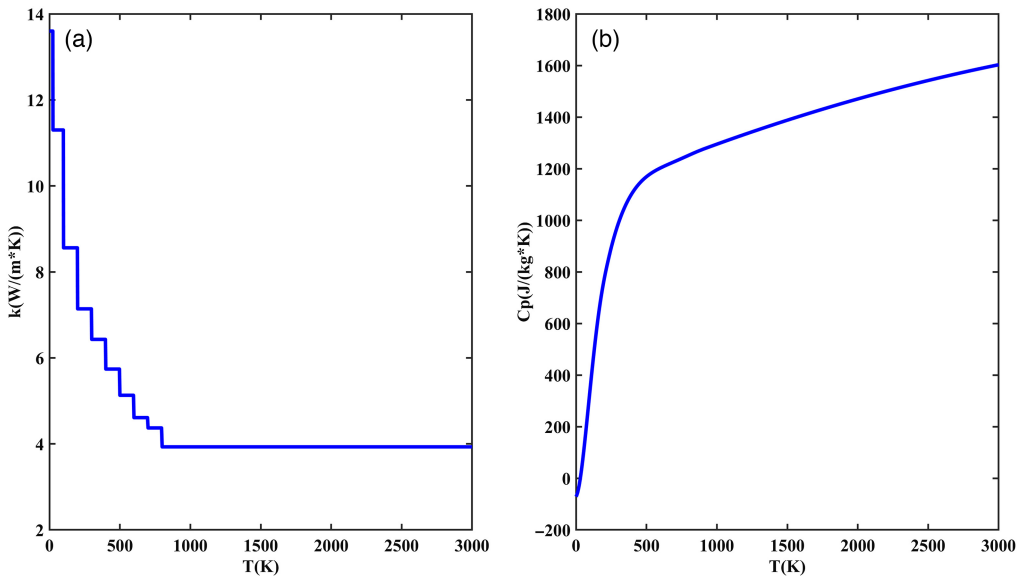

Fig. 2 Curve of thermophysical parameters of MgF_2 versus temperature. (a) Thermal conductivity coefficient and (b) specific heat capacity.

Figure 4 illustrates the temperature distribution after laser action; it can be observed that the laser irradiates the center of target surface, thus increasing the surface temperature and exhibiting a decreasing distribution from the center to edge. The center temperature increased up to 619 K, but it did not reach the melting point of the material (1528.15 K), indicating no melting damage in the material. The edge temperature was 297 K, not significantly different from the ambient temperature (293.15 K), indicating that the material edge was less affected by laser heating for 10 s.

Figure 5 shows that before the laser was applied, the material was deformed owing to the imposition of fixed constraints on its sides. The blue area in Fig. 5(a) indicates that the deformation was smaller than that in the unconstrained part due to fixed restriction. After 10 s of laser action, thermal deformation was observed owing to the absorption of laser energy by the material, resulting in a maximum displacement of 0.04 mm and maximum deformation occurs at material edge. It should be noted that MgF_2 is a brittle material; according to the first strength

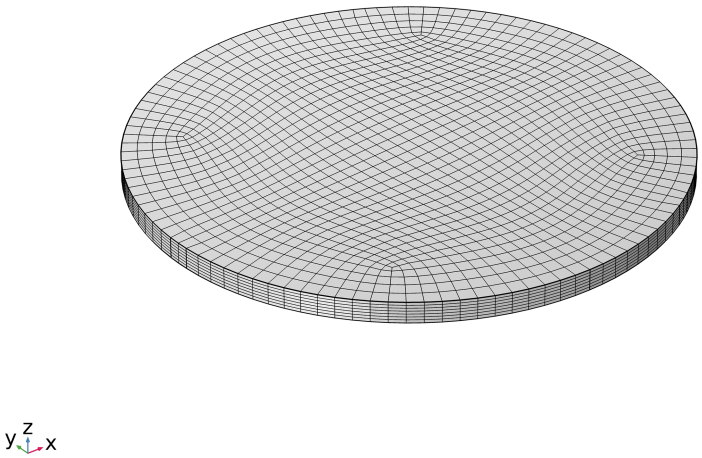

Fig. 3 Grid subdivision of simulation model.

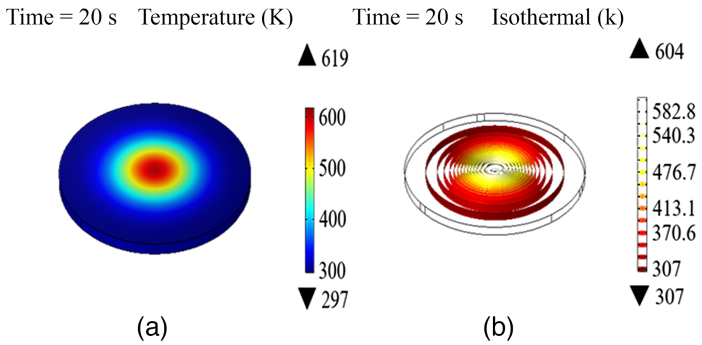

Fig. 4 (a) Temperature distribution at the end of laser action and (b) isothermal distribution at the end of laser action.

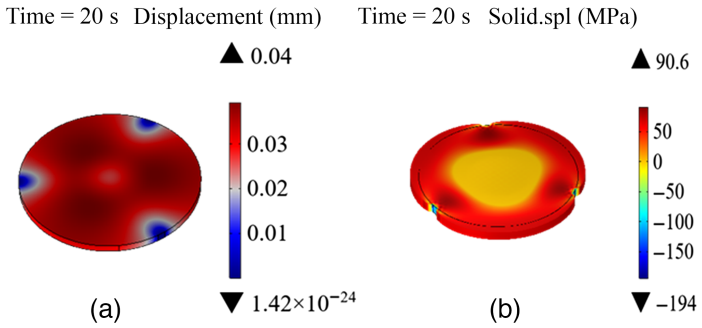

Fig. 5 (a) Thermal deformation after laser action and (b) principal stress after laser action.

theory, damage in brittle materials can be mainly attributed to the maximum tensile stress. When the maximum tensile stress is reached, a point of tensile fracture is observed, which leads to rupture of the material; then, the material is considered to have failed. Figure 5(b) shows the material fracture evaluation criterion; the material fractures when the first principal stress exceeds 49.6 MPa. When the laser was not irradiated, the principal stress of the material was around 0 MPa; when the laser was irradiated, the principal stress of the material became 90.6 MPa, which is greater than the material breaking strength, indicating that the material broke. The largest first principal stress was observed at the material edge; thus, it can be inferred that the material demonstrated burst damage and the crack extended from the edge to center.

Figure 6 shows the evolution process of temperature, displacement, and thermal stress with temperature. When the laser is not applied, the temperature, displacement, and thermal stress do not change. During laser irradiation from 10 to 20 s, the values of aforementioned parameters

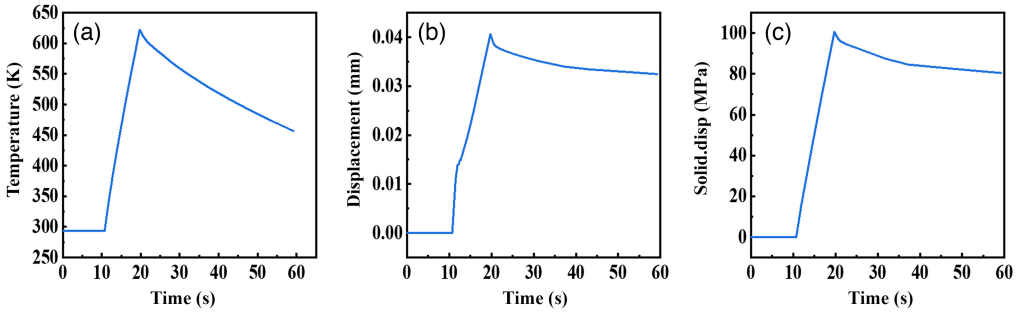

Fig. 6 Thermodynamic effects of MgF_2 under 100 W/cm^2 laser power density irradiation. (a) Temperature evolution with time, (b) displacement evolution with time, and (c) thermal stress evolution with time.

significantly increased. The maximum values of these parameters were obtained when laser irradiation was stopped at 20 s, indicating that the material was not in equilibrium during the irradiation process. The temperature, displacement, and thermal stress values continued to increase. After laser irradiation, these parameters exhibited a downward trend, but the displacement and thermal stress tended to be in equilibrium. For the temperature, no new thermal equilibrium was established inside the material, and gradually, its value decreased. More importantly, Fig. 5(b) demonstrates that the first principal stress of the material reached its breaking strength during the laser action process. Figure 6(c) shows that the material broke at 14.921 s. When the laser irradiated the material with a power density of 100 W/cm^2 for 4.921 s, the material underwent fracture damage due to thermal stress. At this point, the temperature was 439.897 K lower than the melting point of the material (1528.15 K). No melting damage was observed, and the material was considered to have failed.

4.2 Influence of Parameters on Damage Effect

To reveal the damage mechanism of MgF_2 windows under 1.06 μm continuous laser irradiation, we thoroughly analyzed the influence of various factors on the laser damage effect by changing various variables, such as the laser power density, spot size, and action time.

4.2.1 *Power density*

Single-crystal MgF_2 material with a thickness and diameter of 4 and 100 mm, respectively, was irradiated with a 1 μm continuous laser for 10 s. During the laser irradiation process, the temperature and stress of the sample changed with time. The observation and laser action time were 60 and 10 to 20 s, respectively. Moreover, we analyzed the influence of thermodynamic behavior change in other samples by changing the laser power density under other conditions.

When the laser spot radius and irradiation time were 20 mm and 10 s, respectively, the laser power was changed to 628.3, 1256.6, 1885, 2513.3, 3141.6, and 3769.9 W, corresponding to a laser power density of 50, 100, 150, 200, 250, and 300 W/cm^2, respectively. Figure 7 shows the

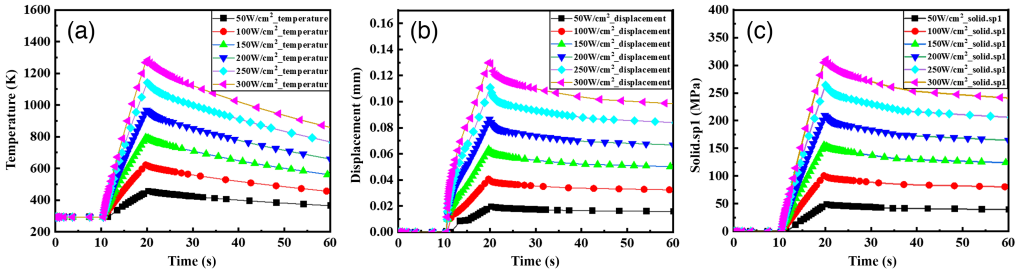

Fig. 7 Thermodynamic effects of MgF_2 under different laser power density irradiation. (a) Temperature evolution with time, (b) displacement evolution with time, and (c) thermal stress evolution with time.

simulation results of the evolution of temperature, displacement, and thermal stress with time when the laser acted on the single-crystal MgF_2 material under different power densities. The laws of the three graphs were found to be similar; the higher the power density, the faster the temperature, displacement, and thermal stress rise. Under the action of a 50 W/cm^2 laser, the maximum principal stress was 48.7 MPa, which did not exceed the fracture limit of the material. The maximum temperature under the action of a 300 W/cm^2 laser was 1284 K, but the principal stress was significantly over the fracture limit, indicating that the material burst. This is because magnesium fluoride cannot absorb the laser heat in time to transfer. In the laser spot irradiation area, the local temperature rises sharply, and a large temperature difference thermal stress is generated in the material. When the thermal stress exceeds the fracture limit of the material, cracks or fractures will occur. The above simulation results indicate that under the same laser power density, the stress damage of Magnesium fluoride material fracture precedes the thermal damage caused by melting. The simulation results are similar to the experimental research results of Qi et al. proving the effectiveness of the simulation model.[13]

4.2.2 *Spot size*

Ignoring the influence of the defects of MgF_2 crystal material, the radius of laser spot acting on the MgF_2 crystal was is 10, 30, and 50 mm with a laser power density of 50, 100, and 200 W/cm^2, respectively, and action time of 10 s. Figures 8(a)–8(f) illustrate the temperature and stress distributions at 50, 100, and 200 W/cm^2, respectively. It can be observed that under the aforementioned laser power densities, the temperature did not exceed the melting point. Even at the same power density, when the light spot was expanded, significant differences were observed in the internal temperature and stress of the material. Figures 8(a) and 8(b) show that only under a power density and spot size of 50 W/cm^2 and 10 mm, respectively, the corresponding maximum stress did not exceed the fracture limit. When the light spot became 30 and 50 mm, the material stress exceeded its fracture limit during laser irradiation.

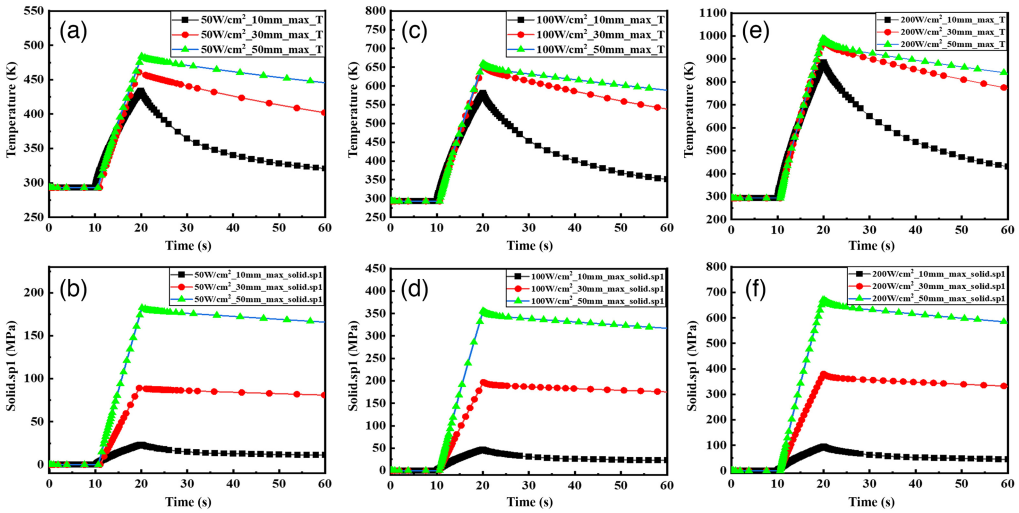

Fig. 8 Evolution of temperature and thermal stress with time for different laser spot sizes. (a) Temperature evolution under a power density 50 W/cm^2 and spot size of 10 mm, 30 mm, and 50 mm. (b) Thermal stress evolution under a power density 50 W/cm^2 and spot size of 10 mm, 30 mm, and 50 mm. (c) Temperature evolution under a power density 100 W/cm^2 and spot size of 10 mm, 30 mm, and 50 mm. (d) Thermal stress evolution under a power density 100 W/cm^2 and spot size of 10 mm, 30 mm, and 50 mm. (e) Temperature evolution under a power density 200 W/cm^2 and spot size of 10 mm, 30 mm, and 50 mm. (f) Thermal stress evolution under a power density 200 W/cm^2 and spot size of 10 mm, 30 mm, and 50 mm.

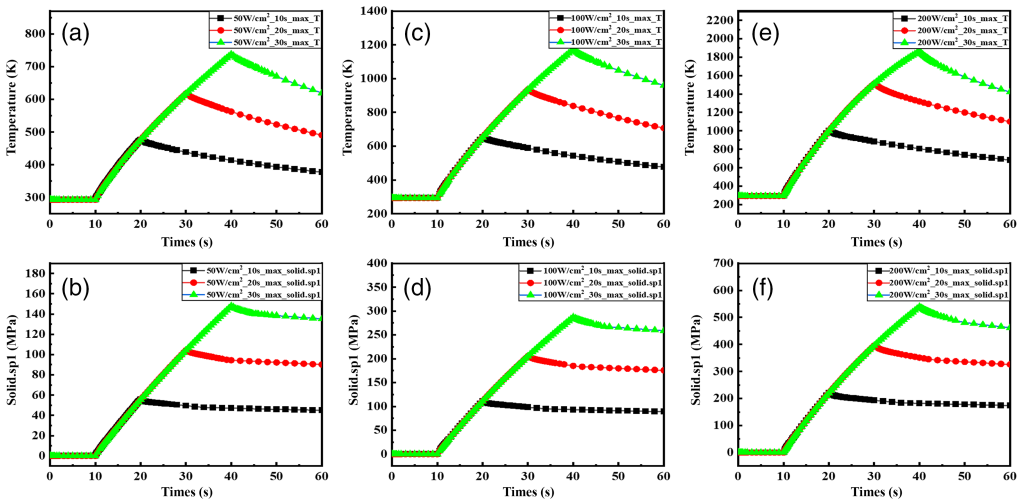

Fig. 9 Evolution of temperature and thermal stress with time for different laser action time. (a) Temperature evolution of 50 W/cm^2 laser for 10 s, 20 s, and 30 s. (b) Thermal stress evolution of 50 W/cm^2 laser for 10 s, 20 s, and 30 s. (c) Temperature evolution of 100 W/cm^2 laser for 10 s, 20 s, and 30 s. (d) Thermal stress evolution of 100 W/cm^2 laser for 10 s, 20 s, and 30 s. (e) Temperature evolution of 200 W/cm^2 laser for 10 s, 20 s, and 30 s. (f) Thermal stress evolution of 200 W/cm^2 laser for 10 s, 20 s, and 30 s.

4.2.3 *Action time*

We explored the effect of laser irradiation time on the thermal damage in single-crystal MgF_2 materials. Accordingly, temperature and stress distribution diagrams were simulated for a laser power density of 50, 100, and 200 W/cm^2, with an action time of 10, 20, and 30 s, respectively.

As shown in Fig. 9, as the laser action time was increased, the material absorbed more laser energy, and the temperature and stress continued to increase until the end of laser action. In addition, compared to Fig. 7(a), Fig. 9(e) shows that when the 300 W/cm^2 laser was applied for 10 s, the maximum temperature rise in the material was 1283 K, which did not reach the melting point (1528.15 K). If the laser heating time was extended to 20 s, the material temperature would have reached the melting point and led to damage under a laser power density of 200 W/cm^2. This shows that even at low laser energy density, the MgF_2 window mirror will be damaged by prolonging the action time.

5 Conclusions

In this study, a finite element software was used to numerically simulate the thermal-mechanical coupling process of high-power fiber laser-irradiated MgF_2 windows. The three-point clamping method demonstrated a significant impact on thermal stress distribution. When a high-power near-infrared continuous laser with a power density and spot diameter of 100 W/cm^2 and 20 mm, respectively, irradiated a single-crystal MgF_2 window with a thickness and diameter of 4 and 100 mm, respectively, for 4.921 s, the thermal stress in the MgF_2 window exceeded the fracture. The strength was 49.6 MPa, and a burst was observed. At this time, the material temperature was 1528.15 K; the melting point of MgF_2 was not reached and no melting damage occurred. In the three-point clamping method, under the same irradiation conditions, the burst damage in MgF_2 material due to thermal stress preceded the melting damage. Using the parameter scanning method, we changed certain parameters, such as the laser power density, spot size, and laser action time. The aforementioned factors demonstrated a significant impact on the thermal damage effect of the material. Our research work has important guiding significance for laser damage and laser protection in the field of optoelectronic countermeasures. In the future, in-depth research can continue on new systems of laser action and laser induced thermal deformation.

Code, Data, and Materials Availability

All data in support of the findings of this paper are available within the article.

Acknowledgments

The work was supported by the Major Innovation Project of CIOMP, CAS (Grant No. E10302Y3M0), National Natural Science Foundation (Grant No. 61904178), Member of the Youth Innovation Promotion Association of the Chinese Academy of Sciences (Grant No. 2020227), and Funding of "Xuguang Talents" from CIOMP.

References

1. Y. Shi et al., "Magnesium fluoride—a summary of the latest data on optical properties," *Laser Optoelectron. Prog.* **12**, 12–13 (1983).
2. L. Wang et al., "Research progress in the application of magnesium fluoride crystals," *Mater. Rev.* **9**, 38–41 (2013).
3. W. Zhang et al., "Review of pulse compression gratings for chirped pulse amplification system," *Opt. Eng.* **60**(2), 020902 (2021).
4. T. A. Van Woerkom et al., "Picosecond laser ablation of metals and semiconductors with low-transverse order Gaussian beams," *Opt. Eng.* **60**(3), 031002 (2020).
5. K. R. P. Kafka et al., "Mechanisms of picosecond laser-induced damage from interaction with model contamination particles on a high reflector," *Opt. Eng.* **60**(3), 031009 (2020).
6. E. Y. K. Cekin et al., "High-power laser-induced optical aberrations on beam director mirrors," *Opt. Eng.* **60**(6), 065102 (2021).
7. G. Yanting et al., "Study on damage of MgF_2 window irradiated by 193 nm ultraviolet excimer laser," *Proc. SPIE* **11912**, 1191203 (2021).
8. J. Wang and G. P. Cox, "ArF laser-induced damage of calcium fluoride windows with protected anti-reflection coatings," *Opt. Eng.* **60**(3), 031007 (2020).
9. J. Ma et al., "Weak absorption and scattering losses from the visible to the near-infrared in single-crystal sapphire materials," *Opt. Eng.* **59**(8), 087101 (2020).
10. E. Migal et al., "Role of wavelength in photocarrier absorption and plasma formation threshold under excitation of dielectrics by high-intensity laser field tunable from visible to mid-IR," *Sci. Rep.* **10**, 14007 (2023).
11. D. Chen et al., "Analytical analysis of heat transfer and thermal stress cracking of window material targets under high-power laser irradiation," *High Power Laser Part Beams* **8**(4), 595–601 (1996).
12. S. Liu et al., "Experimental study of Ge, MgF_2 polycrystals radiated by pulsed laser," *Infrared Laser Eng.* **2**, 25–32 (1994).
13. H. Qi et al., "Destructive effect of 10.6 μm continuous wave laser on MgF_2 materials," *Appl. Laser* **17**(5), 223–224 (1997).
14. W. Wang et al., "Thermal deformation of optical windows irradiated by high power laser beam," *Laser Technol.* **29**(5), 452–458 (2005).
15. H. Sun et al., "Mechanisms of femtosecond laser-induced damage in magnesium fluoride," *Solid State Commun.* **141**(3), 127–131 (2007).
16. Z. Lou et al., "Modeling for the thermal stress damage of the optical elements induced by high energy laser," *Proc. SPIE* **10847**, 108470M (2018).
17. K. Kato et al., "The direct absorption measurement of fused silica, CaF_2, MgF_2, and sapphire at VUV and IR region," *Proc. SPIE* **11173**, 111731K (2019).
18. L. Andrus et al., "Thermal lensing effects and nonlinear refractive indices of fluoride crystals induced by high-power ultrafast lasers," *Appl. Opt.* **59**(28), 8806–8813 (2020).
19. E. Migal et al., "Role of wavelength in photocarrier absorption and plasma formation threshold under excitation of dielectrics by high-intensity laser field tunable from visible to mid-IR," *Sci. Rep.* **10**(1), 14007 (2020).
20. L. Yang et al., "Experimental study on the damage of optical materials by out of band composite laser," *Appl. Sci.* **10**(10), 3578 (2020).
21. W. Jia-min et al., "Damage characteristics of a 532 nm picosecond pulse laser on monocrystalline silicon," *Chin. Opt.* **15**(2), 242–250 (2022).
22. Z. Kuo et al., "Analysis on thermal performance of output window in high power CO_2 laser," *Infrared Laser Eng.* **46**(2), 6 (2017).

Jiamin Wang received her bachelor's degree from Inner Mongolia University in 2018. She is now a PhD student at Changchun Institute of Optics, Precision Mechanics and Physics, Chinese Academy of Sciences. She is mainly involved in research on laser-matter interactions.

Kuo Zhang received his PhD from Jilin University in 2012. He is now an associate researcher and master's supervisor of Changchun Institute of Optics, Precision Mechanics and Physics, Chinese Academy of Sciences. He is mainly engaged in the research of high-power laser technology, laser and matter interaction, etc.

Jinghua Yu received his MD from the Chinese Academy of Sciences Changchun Institute of Optics, Precision Mechanics and Physics. He currently works at the Chinese Academy of Sciences Changchun Institute of Optics, Precision Mechanics and Physics. He is mainly engaged in the research of ultrafast lasers.

Yi Chen received his PhD from Harbin Institute of Technology. He is currently an engineer at Changchun Institute of Optics, Precision Mechanics and Physics, Chinese Academy of Sciences. He is mainly engaged in the research of disc laser technology and long wave infrared laser.

Changbin Zheng received his PhD from Harbin Institute of Technology. He is an associate researcher at Changchun Institute of Optics, Precision Mechanics and Physics, Chinese Academy of Sciences. He is mainly engaged in the interaction between laser and matter.

Peng Yang received his bachelor's degree from the School of Ordnance Engineering and received his MD from the Army University of Engineering. His main research field is optoelectronic equipment testing.

Guohui Bao received his bachelor's degree from the University of Electronic Science and Technology. He is mainly engaged in optoelectronics and optoelectronic countermeasures.

Fei Chen received his PhD from the Harbin Institute of Technology in 2011. Currently, he is a doctoral supervisor and researcher at Changchun Institute of Optics, Precision Mechanics and Physics, Chinese Academy of Sciences. His research interests include new laser technologies and applications research.